

Application of Markov Structure of Genomes to Outlier Identification and Read Classification

Alan F. Karr*, Jason Hauzel†, Adam A. Porter‡, Marcel Schaefer§

December 28, 2021

Abstract

In this paper we apply the structure of genomes as second-order Markov processes specified by the distributions of successive triplets of bases to two bioinformatics problems: identification of outliers in genome databases and read classification in metagenomics, using real coronavirus and adenovirus data.

1 Introduction

That the sequential structure of genomes is important has been known since the discovery of DNA. In this paper we employ a statistics and stochastic process perspective on triplets of successive bases to address two important applications: identifying outliers in genome databases, and classifying reads in the metagenomic context of reference-guided assembly. From this stochastic process perspective, triplets are a second-order Markov chain specified by the distribution of each base conditional on its two immediate predecessors.

To be sure, studying genomes via base sequence distributions is not novel. Previous papers have addressed genome signatures (Karlin et al., 1997; Campbell et al., 1999; Takashi et al., 2003), as well as frequentist (Rosen et al., 2008) and Bayesian (Wang et al., 2007) approaches to classification problems. While we focus instead on triplet distributions, many extant works employ quartets, also referred to as tetranucleotides, among them Pride et al. (2003), Teeling et al. (2004a) and Teeling et al. (2004b).

In §3, we apply hierarchical cluster analysis of triplet distributions to identification of outliers in genome databases. Genomes in small or highly divergent clusters are statistical outliers. They may be data quality problems, as some in our example clearly are, or simply aberrant. The clustering is both statistically effective and scientifically interpretable.

The second application, in §4, is Bayesian classification of (short) reads in metagenomics. The latter has consequences for uncertainty quantification, in particular allowing assessment of the contributions to uncertainty of prior knowledge, input data quality, and training data quality, which is also interpretable as model quality. Throughout, we use real data, primarily a coronavirus dataset downloaded from the National Center for Biotechnology Information (NCBI), as well as a single adenovirus genome included in the download package for the Art read simulator (Huang et al., 2012). Each genome has length on the order of 30,000 base pairs (BP), representing approximately 20 genes. Conclusions appear in §5.

*Fraunhofer USA CMA; akarr@fraunhofer.org; Corresponding author

†Fraunhofer USA CMA; jhauzel@fraunhofer.org

‡University of Maryland, Department of Computer Science; aporter@cs.umd.edu

§Fraunhofer USA CMA; mschaefer@fraunhofer.org

2 Background

In this paper, a genome G is a character string chosen from the base (nucleotide) alphabet $\mathcal{B} = \{A, C, G, T\}$, and represents one strand of the DNA in an organism. Given a genome G , the length of G is $|G|$; the i^{th} base in G is $G(i)$; and the bases from location i to location $j > i$ are $G(i : j)$. For $n \geq 1$, let $\mathcal{B}(n)$ be the set of all sequences of length n from \mathcal{B} , of which there are 4^n . We focus on triplets, whose distributions are 64-dimensional summaries of genomes;¹ for this focal case, $\mathcal{B}(3) = \{AAA, AAC, \dots, TTG, TTT\}$, and the triplet distribution $P_3(\cdot|G)$ is defined as

$$P_3(b_1b_2b_3|G) = \text{Prob}\{G(k : k + 2) = b_1b_2b_3\} \quad (1)$$

for each choice of b_1, b_2, b_3 from \mathcal{B} , where k is chosen at random from $1, \dots, |G| - 2$. An equivalent perspective is that of a second-order Markov chain. The information contained in $P_3(\cdot|G)$ is the same as that contained in the pair distribution $P_2(\cdot|G)$ and the 16×4 transition matrix

$$T_3((b_1, b_2), b_3|G) = \text{Prob}\{G(k + 2) = b_3 | G(k) = b_1, G(k + 1) = b_2\}, \quad (2)$$

whose rows are indexed by (b_1, b_2) and columns are indexed by b_3 , and which gives the distribution of each base conditional on its two predecessors.

Appendix A contains examples of both distributions for the three virus genomes underlying the read classification problem in §4.

3 Outlier Detection

In this section, we use triplet and amino acid distributions to detect outliers in the NCBI database. Outliers may be true scientific anomalies, or they may be data quality problems (Karr et al., 2021b). That large, uncurated problem genome databases may have quality issues is of increasing concern in a variety of contexts (Biggio and Roli, 2018; Steinegger and Salzberg, 2020; Valdivia-Granda, 2019).

Our strategy is to use hierarchical cluster analysis (Aggarwal and Reddy, 2013; Everitt, 2011) of the 64-dimensional triplet distributions, and then to investigate clusters with small counts, which *are* outliers in a statistical sense, to see if they are outliers in other senses. As our experimental platform, we employ a coronavirus database containing 26,953 genomes, which was downloaded from the NCBI in November of 2020. To it, we added eleven “known” outliers: one adenovirus genome and low-quality versions of ten coronavirus genomes selected randomly from the 26,953. The latter were produced using the degradation methodology described in Karr et al. (2021b), which consists of repeated iterations of the `Mason_variator` haplotype generation software (Holtgrewe, 2010). The clustering was performed on standardized versions of the triplet distributions using the “complete” method for hierarchical clustering (Müllner, 2013) in the R software system (R Core Team, 2020).

We emphasize that some of what follows requires knowledge of the sources of the genomes (original coronavirus dataset, adenovirus or degraded) that is not available in some other contexts.

¹Other cases of interest appear in the literature. Base distributions ($n = 1$) and pair distributions ($n = 2$) are too coarse to be useful for the problems we address. Quartets ($n = 4$) have historical precedent (Pride et al., 2003; Teeling et al., 2004a,b). Based on informal experiments, for the applications in §3 and 4, quartets are more cumbersome computationally than triplets, but do not seem to be significantly more informative.

3.1 Clustering Based on Triplet Distributions

Figure 1 contains results for triplet-based hierarchical clustering in 64 dimensions.² The number of clusters, which is 23, was determined using standard heuristics that trade off complexity for explanatory power. The top panel is a plot of the cluster centroids reduced to two dimensions using multidimensional scaling (MDS) (Kruskal and Wish, 1978; Cox and Cox, 2001). The greater the separation in the plot, the greater the dissimilarity between clusters. The bottom panel of Figure 1 is the associated dendrogram, depicting the dynamics of the clustering process, and is discussed in more detail below.

Statistically, the quality of the clustering is very high. The percentage of the variation of each triplet frequency, over the entire 26,964-genome dataset, that is explained by the cluster numbers alone is very large. Specifically, for each triplet x , a linear model of the form $P_3(x|\cdot) \sim \text{ClusterNumber}(\cdot)$ was fitted, treating the latter as a categorical variable. All of the coefficients of determination, R^2 , exceed 0.93, and the majority exceed 0.98.

Table 1 complements the dendrogram in Figure 1. In the dendrogram, the x -axis, *Height*, is the stage in the clustering process at which splits occur; the greater the height, the earlier the split. So, for example, the first split in the dendrogram creates two branches, the upper one containing the eleven added outliers and one coronavirus genome, and the lower containing the remaining 26,952 coronavirus genomes. Although this is not a logical necessity, every final cluster contains only one “kind” of genome, labeled *Class*, which appears in the MDS plot, the dendrogram and the table.³ *Separation Height* Table 1 is that at which the cluster is separated from all the others and not split further. The higher this value, the earlier in the process a cluster is permanently split off from the others. *Separation Rank* orders the clusters by Separation Height, with the greatest value of height having rank 1. Ties end in .5.

We now interpret. The overwhelming majority of coronavirus genomes—26,433 of the original 26,953, or 98.1%—are in cluster 11. Cluster 13 contains the adenovirus genome alone; each of the 10 degraded coronavirus genomes appears in a cluster by itself (clusters 14–23). Therefore, the deliberate outliers are not only all detected, but also distinguished from one another.⁴ The MDS plot in Figure 1 shows that these 10 degraded coronavirus outliers differ more from the coronavirus genomes (clusters 1–12) and the adenovirus (cluster 13) than from one another. The adenovirus genome differs from both the coronavirus genomes and the degraded coronavirus outliers.

One original coronavirus genome appears by itself, in cluster 12. Without question it is an outlier; as noted above, it is separated from the other coronavirus genomes at the first split. However, we see below that when clustering is based on amino acids instead of triplets, it ceases to be an outlier. The NCBI dataset ID of this genome is *MT451283.1 Severe acute respiratory syndrome coronavirus 2 isolate SARS-CoV-2/human/AUS/VIC402/2020, complete genome*. No other genome ID in the database is similar to it, which we take as scientific confirmation that the triplet distribution-based clustering truly detects outliers.

Cluster 16 has Separation Rank 1: that particular degraded coronavirus genome is the first to be separated permanently from everything else. Cluster 12, with the singleton outlier coronavirus genome, is second. Of the remaining clusters (1–10), cluster 1 is the strongest candidate for containing outliers. Not only does it have Separation Rank 3, but also its count is small. The next two highest ranked coronavirus clusters (4 and 7) do not have similarly small counts, but based on the results here and in §3.2 are nevertheless compelling candidates to be outliers.

²Technically, in a 63-dimensional hyperplane, since the 64 probabilities sum to one.

³“Kind” was termed source previously, and is one of coronavirus, adenovirus or degraded coronavirus.

⁴We caution against over-interpretation. Some of the behavior is a consequence of the small number of deliberate outliers.

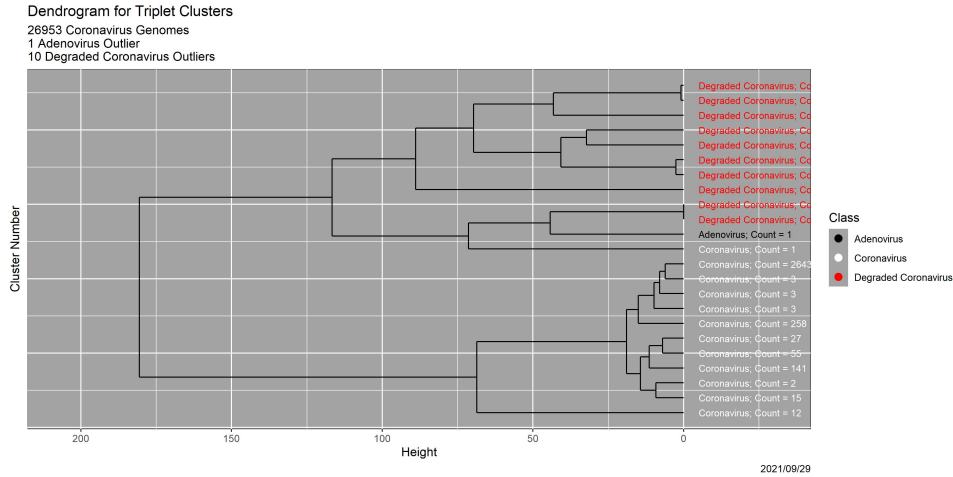
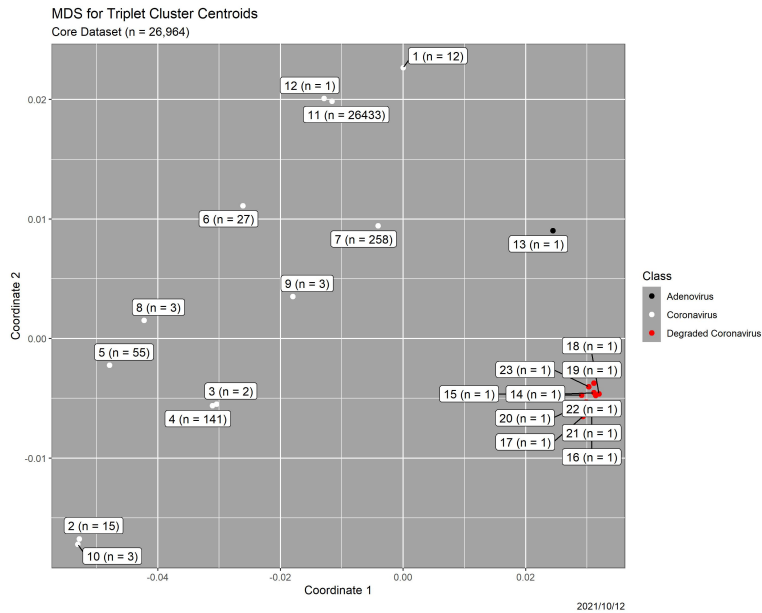


Figure 1: *Top*: Two-dimensional MDS plot of triplet distribution of cluster centroids for the 26,964-element coronavirus dataset containing 26,953 coronavirus genomes and 11 deliberately added outliers. *Bottom*: Corresponding dendrogram. Class in both plots is the same as in Table 1, and is shown in the same colors in both graphics.

Cluster	Count	Class	Separation Height	Separation Rank
1	12	Coronavirus	68.60	3
2	15	Coronavirus	9.23	11.5
3	2	Coronavirus	9.23	11.5
4	141	Coronavirus	11.42	9
5	55	Coronavirus	6.98	14.5
6	27	Coronavirus	6.98	14.5
7	258	Coronavirus	15.03	8
8	3	Coronavirus	9.87	10
9	3	Coronavirus	7.99	13
10	3	Coronavirus	6.08	16.5
11	26433	Coronavirus	6.08	16.5
12	1	Coronavirus	71.43	2
13	1	Adenovirus	44.29	4
14	1	Degraded Coronavirus	0.00	22.5
15	1	Degraded Coronavirus	0.00	22.5
16	1	Degraded Coronavirus	88.92	1
17	1	Degraded Coronavirus	2.58	18.5
18	1	Degraded Coronavirus	2.58	18.5
19	1	Degraded Coronavirus	32.20	6.5
20	1	Degraded Coronavirus	32.20	6.5
21	1	Degraded Coronavirus	43.27	5
22	1	Degraded Coronavirus	0.92	20.5
23	1	Degraded Coronavirus	0.92	20.5

Table 1: Characteristics of the triplet distribution clusters in Figure 1. See text for explanation of Separation Height and Separation Rank. The double horizontal line divides original 26,953 coronavirus genomes from the 11 deliberate outliers.

Returning to the ID-based interpretation of cluster 12, Table 2 shows that every coronavirus cluster 1–10 (i.e., all except the the outlier constituting cluster 12 and the cluster with 26,433 members) is essentially defined by a substring of the ID, subject to two qualifications. First, some clusters (to wit, 1, 4, and 7) contain multiple substrings that cover the cluster and appear in no other cluster. And second, there are substrings that cover multiple clusters but appear in no other clusters. For instance, “Human coronavirus HKU1” covers all 15 elements of cluster 2 and all 3 elements of cluster 10, and appears nowhere else. We again conclude that the clustering captures scientific reality.

3.2 Clustering Based on Amino Acids

Clustering was also performed on amino acid distributions,⁵ in 21 dimensions rather than 64, resulting in the MDS plot and dendrogram shown in Figure 2 and the cluster characteristics in Table 3. There are fewer

⁵Generated directly from triplet distributions using the known many-to-one mapping of triplets to amino acids.

Cluster	Cluster Count	Substring of ID	Count in	
			This Cluster	Other Clusters
1	12	TOTAL		
		SARS coronavirus Tor2	2	0
		SARS coronavirus GDH-BJH01	1	0
		SARS coronavirus P2	1	0
		SARS coronavirus HKU-39849 isolate TCVSP-HARROD	2	0
		SARS coronavirus Urbani isolate icSARS	6	0
2	15	Human coronavirus HKU1	15	3
			3	15
3	2	Human enteric coronavirus [...] 4408	2	0
4	141	TOTAL		
		Human coronavirus OC43 strain	138	0
		Coronavirus cy[abc]-BetaCoV/2019	3	0
5	55	Human coronavirus NL63 strain	55	6
			3	58
			3	58
6	27	Human coronavirus 229E	27	0
7	258	TOTAL		
		Middle East respiratory syndrome	253	0
		[Bb]etacoronavirus	5	0
12	1	SARS-CoV-2/human/AUS/VIC402/2020	1	0

Table 2: Substrings of NCBI IDs that characterize the clusters containing coronavirus genomes. Single-member clusters comprised of the adenovirus genome or one of the ten degraded coronavirus genomes are excluded.

clusters than for triplets—13 as compared to 23. The statistical explanatory power matches that for triplets: all coefficients of determination exceed 0.95.

Table 4, a cross-tabulation of triplet distribution clusters (rows) and amino acid distribution clusters (columns), shows that each amino acid cluster is either identical to a triplet distribution cluster or an amalgam of triplet distribution clusters. Specifically, for the deliberate outliers, the adenovirus genome remains in a cluster of its own (13 for triplets; 10 for amino acids), while the 10 degraded coronavirus genomes (triplet clusters 14–23) are condensed to three amino acid clusters (11–13). Interestingly, the coronavirus genome that alone comprised triplet cluster 12 is absorbed into the massive cluster (triplet cluster 11), which now has size 26,434 (amino acid cluster 9). Triplet cluster 1 (count = 12) and amino acid cluster 1 are identical, as are triplet cluster 5 (count = 55) and amino acid cluster 12, as well as triplet cluster 6 (count = 27) and amino acid cluster 5, triplet cluster 7 (count = 258) and amino acid cluster 6, triplet cluster 8 (count = 3) and amino acid cluster 7 and, finally, triplet cluster 9 (count = 3) and amino acid cluster 10. Triplet clusters 2 and 10 are merged to create amino acid cluster 2, while triplet clusters 3 and 4 merge into amino acid cluster 3.

The dendrogram in Figure 2 and the separation heights and ranks in Table 3 add insightful nuances. In the dendrogram, the first split isolates amino acid clusters 1–4 from everything else, including the massive coronavirus cluster and the deliberate outliers. The next split isolates the ten degraded coronavirus genomes from the latter, but the adenovirus genome remains coupled with the dominant coronavirus cluster until relatively late in the process (height = 7.2), which is the separation height for both. Ignoring the deliberate outliers, there are two extreme separation heights—34.9 for cluster 5 and 33.0 for cluster 1. The latter reinforces our hypothesis in §3.1 that cluster 1 contains outliers. The analogous message regarding cluster

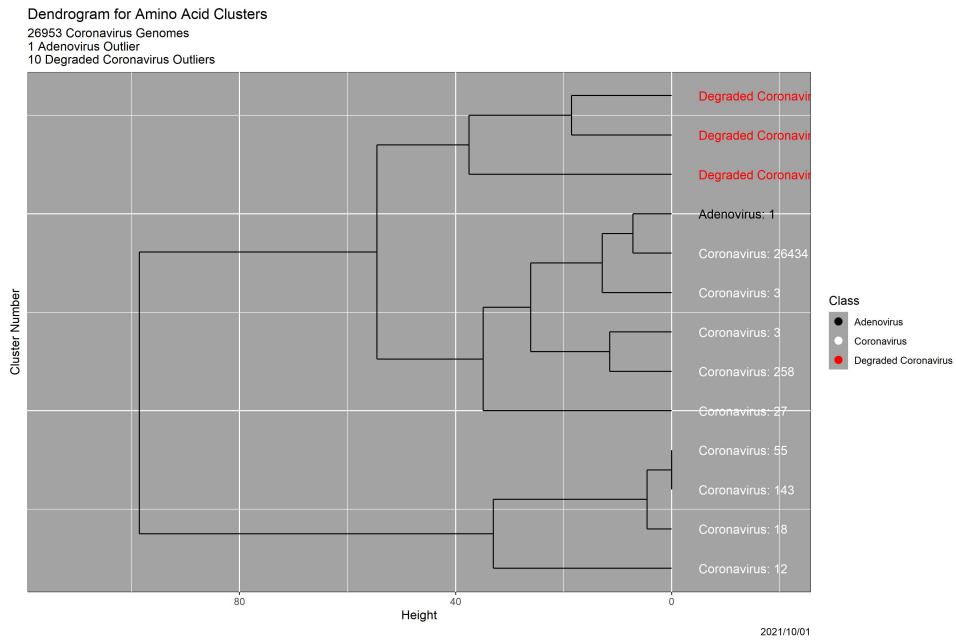
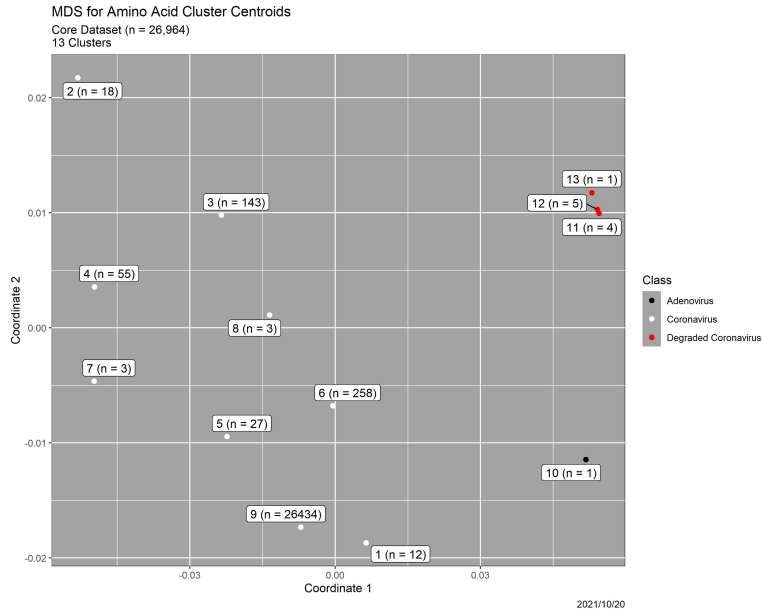


Figure 2: *Top*: Two-dimensional MDS plot of amino acid distribution of cluster centroids for the 26,964-element coronavirus dataset containing 26,953 coronavirus genomes and 11 deliberately added outliers. *Bottom*: Corresponding dendrogram. Class in the dendrogram is the same as in Table 3, and shown the the same colors in both graphics.

Cluster	Count	Class	Separation Height	Separation Rank
1	12	Coronavirus	33.0	3.0
2	18	Coronavirus	4.6	11.0
3	143	Coronavirus	0.0	12.5
4	55	Coronavirus	0.0	12.5
5	27	Coronavirus	34.9	2.0
6	258	Coronavirus	11.5	7.5
7	3	Coronavirus	11.5	7.5
8	3	Coronavirus	12.8	6.0
9	26434	Coronavirus	7.2	9.5
<hr/> <hr/>				
10	1	Adenovirus	7.2	9.5
11	4	Degraded Coronavirus	37.5	1.0
12	5	Degraded Coronavirus	18.5	4.5
13	1	Degraded Coronavirus	18.5	4.5

Table 3: Characteristics of the amino acid distribution clusters in Figure 2. See text for explanation of Separation Height and Separation Rank. The double horizontal line divides coronavirus genomes from the deliberate outliers.

Triplet Cluster	Amino Acid Cluster													Sum
	1	2	3	4	5	6	7	8	9	10	11	12	13	
1	12	0	0	0	0	0	0	0	0	0	0	0	0	12
2	0	15	0	0	0	0	0	0	0	0	0	0	0	15
3	0	0	2	0	0	0	0	0	0	0	0	0	0	2
4	0	0	141	0	0	0	0	0	0	0	0	0	0	141
5	0	0	0	55	0	0	0	0	0	0	0	0	0	55
6	0	0	0	0	27	0	0	0	0	0	0	0	0	27
7	0	0	0	0	0	258	0	0	0	0	0	0	0	258
8	0	0	0	0	0	0	3	0	0	0	0	0	0	3
9	0	0	0	0	0	0	0	3	0	0	0	0	0	3
10	0	3	0	0	0	0	0	0	0	0	0	0	0	3
11	0	0	0	0	0	0	0	0	26433	0	0	0	0	26433
12	0	0	0	0	0	0	0	0	1	0	0	0	0	1
13	0	0	0	0	0	0	0	0	0	1	0	0	0	1
14	0	0	0	0	0	0	0	0	0	0	1	0	0	1
15	0	0	0	0	0	0	0	0	0	0	0	1	0	1
16	0	0	0	0	0	0	0	0	0	0	0	0	1	1
17	0	0	0	0	0	0	0	0	0	0	0	1	0	1
18	0	0	0	0	0	0	0	0	0	0	0	1	0	1
19	0	0	0	0	0	0	0	0	0	0	0	1	0	1
20	0	0	0	0	0	0	0	0	0	0	1	0	0	1
21	0	0	0	0	0	0	0	0	0	0	1	0	0	1
22	0	0	0	0	0	0	0	0	0	0	1	0	0	1
23	0	0	0	0	0	0	0	0	0	0	0	1	0	1
Sum	12	18	143	55	27	258	3	3	26434	1	4	5	1	26964

Table 4: Cross-tabulation of triplet-based clusters and amino acid-based clusters. Entries corresponding to identical clusters are highlighted in **enlarged boldface**.

5 is attenuated, so using amino acids provides information not available from triplets alone. The very last split in the amino acid dendrogram, which separates cluster 3 (count = 143) and cluster 4 (count = 55) is less discernible in the dendrogram in Figure 1.

4 Bayesian Classification of Simulated Illumina Reads

In this section, we apply triplet distributions to the metagenomics problem of classifying short genome reads in mixtures comprising multiple genomes, a common step in reference-guided assembly.

4.1 The Experiment

The components of the experiment are introduced here.

Reference Genomes. There are three reference genomes: the adenovirus genome of length 34,125, downloaded with the read simulator `Art`, which we also call Adeno; a SARS-CoV-2 genome of length 29,926 contained in the NCBI coronavirus dataset employed in §3, which we call COVID; and a severe acute respiratory syndrome (SARS) genome of length 29,751 from the same database, which we call SARS. Tables 10 and 11, in Appendix A, show the triplet and amino acid distributions for these three genomes. A natural question is “How different are these triplet distributions?” Measured by Hellinger distance (Nikulin, 2001) they are very different. The distances are 0.234 for adenovirus/COVID, 0.125 for adenovirus/SARS and 0.161 for COVID/SARS. To gauge these differences, the empirical 0.001 p -values for distributions of genomes of the same size simulated from each distribution are 0.01941755 for adenovirus, 0.02094808 for COVID, and 0.02065539 for SARS. The Hellinger distances for amino acid distributions are 0.189 for adenovirus/COVID, 0.090 for adenovirus/SARS and 0.130 for COVID/SARS. All these distances exceed empirical 0.1% p -values.

Read Generation. The `Mason_simulator` read simulator (Holtgrewe, 2010) was used to simulate Illumina⁶ reads of length 101 from each genome, with approximate 6X coverage. The numbers of reads are 1966, 1996 and 1907, respectively; the total number of reads is 5869. The `Mason_simulator` introduces errors in the form of transpositions (single nucleotide polymorphisms (SNPs)), insertions, deletions and undetermined bases, which, following convention, appear in the simulated reads as “N” and must be accommodated in computation of likelihood functions. Parameters of the `Mason_simulator` were set at default values.

Likelihood Functions. Three likelihood functions, one for each genome and denoted by $L_A(\cdot)$, $L_C(\cdot)$ and $L_S(\cdot)$, were calculated, representing the triplet distributions. To illustrate for adenovirus,

$$L_A(R) = P_2(R(1)R(2)|A) \times T_3((R(1), R(2)), R(3)|A) \\ \times T_3((R(2), R(3)), R(4)|A) \times \cdots \times T_3\left((R(|R| - 2), R(|R| - 1)), R(|R|)|A\right), \quad (3)$$

where $R(k)$ is the k^{th} element of the read R , $P_2(\cdot|A)$ is the pair distribution, and T_3 is given by (2). In (3), we have ignored Ns for simplicity; when they are present, they lead to sums over all possible bases. Below, we also explore alternative likelihood functions representing deliberate degradation of quality of the training data by means of the `Mason_variator`.

⁶Illumina is a major manufacturer of high-end instruments for genome sequencing; their technology is optical in nature; see <https://www.illumina.com/>.

Prior and Posterior Probabilities. For each read R , we specify a prior probability distribution π_R over the set $\mathcal{A} = \{\text{Adeno}, \text{COVID}, \text{SARS}\}$ of the three genomes, and then use Bayes’ theorem and the three likelihoods to calculate posterior probabilities over \mathcal{A} , which we then analyze. Specifically, for each read R , the posterior probability of $x \in \mathcal{A}$ is given by

$$p(x|R) = \frac{\pi_R(x)L_x(R)}{\pi_R(A)L_A(R) + \pi_R(C)L_C(R) + \pi_R(S)L_S(R)}. \quad (4)$$

Experimental Protocol. All three components in the calculation can be varied, and their contributions to the final output resolved:

The input data, that is, the reads themselves, which contain `Mason_simulator`-generated errors. Because the `Mason_simulator` records the starting location of each read, we have as well the error-free reads, which are of higher quality. Conversely, we can use the `Mason_variator` to degrade read quality, as in Karr et al. (2021b).

The prior distributions, which in most cases we take to be (mildly) informative distributions generated randomly from a Dirichlet distribution. An alternative representing no external prior knowledge is the non-informative priors $\pi_R = (1/3, 1/3, 1/3)$.

The models, embedded in the likelihood functions for the three genomes. The three genomes themselves are, in effect, the training data. As discussed further below, model quality can be decreased by degrading them using the `Mason_variator`.

4.2 The Base Case

As base case, we use the informative priors, the actual reads and the correct models based on the triplet distribution likelihood functions from the three genomes. Figure 3 contains the results. Because similar figures follow, we discuss it in some detail. First, three-dimensional probabilities (barycentric coordinates) are represented in the figure using Cartesian coordinates, as points in a two-dimensional simplex—an equilateral triangle. Pure adenovirus, in the sense that $\text{Prob}(\text{Adeno}) = 1$, is the top vertex, pure COVID is the lower left vertex, and pure SARS is the lower right vertex. Because we know the sources of the reads, we create separate displays for each source—adenovirus at the left, COVID in the center and SARS at the right. The upper three panels show prior probabilities, while the lower three panels show posterior probabilities. The green/red/blue coloring depicting read source is redundant, but useful. The white diamond in each scatterplot is the centroid of the probabilities it contains.

The interior black lines, which are often not completely visible, are the decision boundaries for the MAP (maximum *a posteriori* probability) classifier, which assigns to each read the genome with the highest posterior probability. The value of the largest posterior probability cannot be less than 1/3, but can be arbitrarily close to it. Points that lie near any of these boundaries are close calls, but are not distinguished by the MAP classifier from clear-cut cases.⁷ Alternative decision strategies in Karr et al. (2021a) implement a concept known as Specified Certainty Classification (SSC) that enforces a user-specified lower bound on the certainty of each decision.

⁷To note an extreme example, the MAP classifier does not distinguish read R with $p(\cdot|R) = (0.34, 0.33, 0.33)$ —an extremely close call—from read R' with $p(\cdot|R') = (0.99, 0.005, 0.005)$ —a near-certainty to be from the adenovirus genome. In some contexts, this may be problematic.

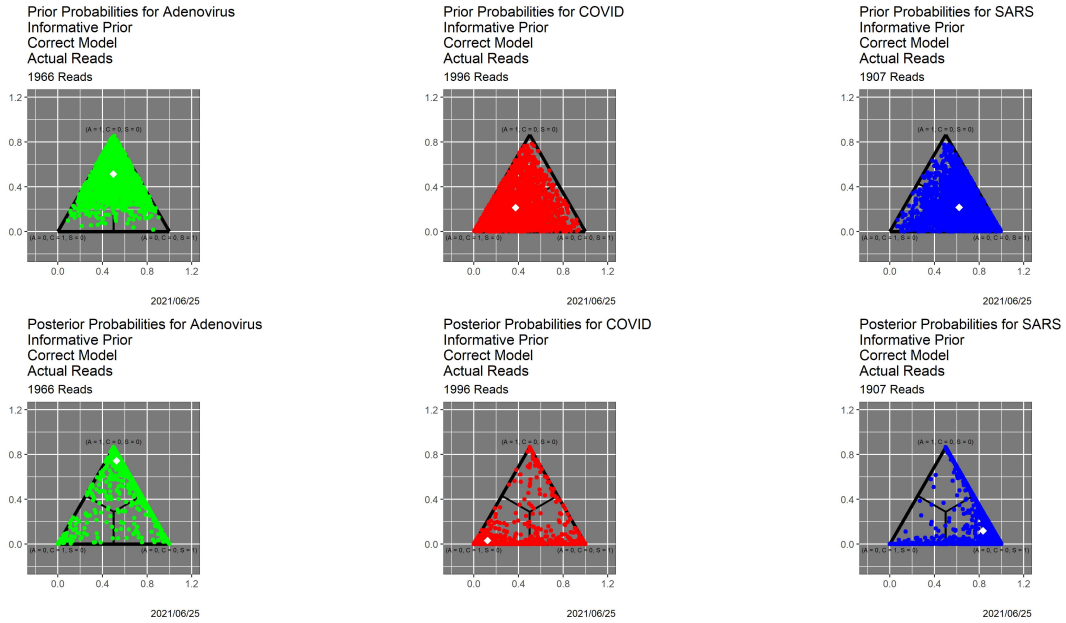


Figure 3: Prior and posterior probabilities for the base case of actual reads, informative prior distributions and correct triplet distribution-based models. *Top left*: Prior probabilities for reads from adenovirus. *Top middle*: Prior probabilities for reads from COVID. *Top right*: Prior probabilities for reads from SARS. *Bottom left*: Posterior probabilities for reads from adenovirus. *Bottom middle*: Posterior probabilities for reads from COVID. *Bottom right*: Posterior probabilities for reads from SARS. White symbols in each plot are centroids.

Now to interpretations. That the prior distributions are informative is manifested in that each, while scattered, gravitates toward the vertex representing the truth. From the prior to the posterior, all probabilities shift in the direction of the truth—which is what data are supposed to do. Centroids move in response. We caution that there is massive overplotting. For instance, the posterior probabilities for adenovirus (lower left) appear scattered, yet the centroid is very close to the truth—the upper vertex. Table 5 shows the base case confusion matrix for the MAP classifier. The performance is imperfect but respectable: the correct classification rate is $(1757 + 1762 + 1549)/5869 = 86.35\%$.

4.3 Variations on the Base Case

In terms of understanding all the decisions the classifier *can make*, as opposed to the decisions it *does make* in a specific application (Karr et al., 2019), the Bayesian framework allows investigation and quantification of the relative contributions to uncertainty of the priors, the data and the models. Here we explore the effect of each.

Changing the Priors. The priors are relatively the least important of the three, with one important *caveat* discussed momentarily. Figure 4 is the analog of Figure 3 for the “no prior knowledge” case that $\pi_R = (1/3, 1/3, 1/3)$ for all reads R . The visual message that there is no dramatic difference is corroborated

Source	Decision			Sum
	Adeno	COVID	SARS	
Adeno	1757	74	135	1966
COVID	64	1762	170	1996
SARS	214	144	1549	1907
Sum	2035	1980	1854	5869

Table 5: Confusion matrix for the MAP classifier for the base case. Rows are read sources; columns are MAP classifier decisions. The correct classification rate is 86.35%.

by the confusion matrix in Table 6; the correct classification rate has declined only modestly, to $(1601 + 1717 + 1470)/5869 = 81.58\%$.

Source	Decision			Sum
	Adeno	COVID	SARS	
Adeno	1601	115	250	1966
COVID	64	1717	215	1996
SARS	268	169	1470	1907
Sum	1933	2001	1935	5869

Table 6: Confusion matrix for the MAP classifier for the case of actual reads, “no knowledge” priors, and correct triplet distribution-based models. The correct classification rate is 81.58%.

Zeros in priors, however, can be highly problematic. The “no adenovirus” priors $\pi_R = (0, 1/2, 1/2)$ instantiate a mistaken belief that no adenovirus reads are present. Figure 5 contains results for these priors, actual reads, and the correct triplet distribution-based models. All posterior probabilities lie on the COVID–SARS axis—the bottom edge of the triangle. Table 7 contains the associated confusion matrix. Because, as (4) makes clear, a zero in a prior distribution is inherited by the posterior, all adenovirus reads are misclassified, most of them as SARS. The operational lesson is that “if it might be there, allow for it in the priors.” See §4.4 for further discussion in the context of contamination.

Hereafter, we consider only the informative priors, and omit prior probabilities from the graphics.

	Decision		Sum
	COVID	SARS	
Adeno	163	1803	1966
COVID	1728	268	1996
SARS	177	1730	1907
Sum	2068	3801	5869

Table 7: Confusion matrix for the MAP classifier for the case of actual reads, “no adenovirus” priors, and correct triplet distribution-based models. The correct classification rate is 58.92%

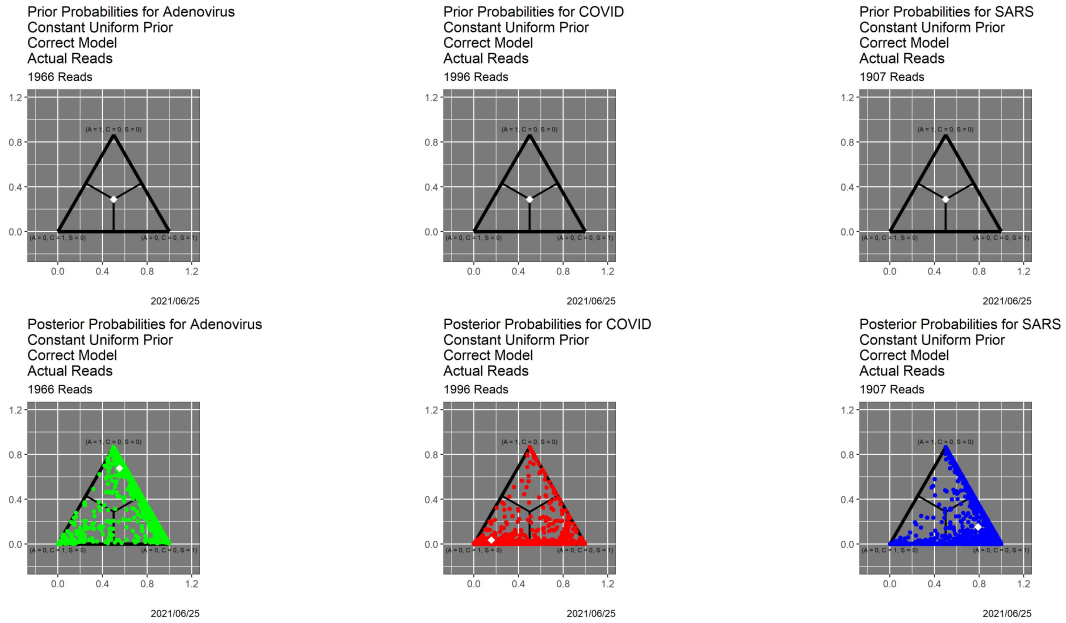


Figure 4: Prior and posterior probabilities for the case of actual reads, “no knowledge priors” and correct triplet distribution-based models. *Top left*: Prior probabilities for reads from adenovirus. *Top middle*: Prior probabilities for reads from COVID. *Top right*: Prior probabilities for reads from SARS. *Bottom left*: Posterior probabilities for reads from adenovirus. *Bottom middle*: Posterior probabilities for reads from COVID. *Bottom right*: Posterior probabilities for reads from SARS. White symbols in each plot are centroids.

Changing Read (= Input Data) Quality. Figure 6 shows the effects of increasing and decreasing the quality of the simulated reads. To enable comparisons, the top panel there is the base case posterior probabilities appearing at the bottom of Figure 3. The middle panel shows that using the error-free reads in place of the `Mason_simulator`-generated reads makes no meaningful difference. This is because the default error rates in the `Mason_simulator` are not large.

More dramatic is the effect of degrading the reads using 1000 iterations of the `Mason_variator`, in the manner of Karr et al. (2021b), which is shown in the bottom panel in Figure 6. The associated MAP confusion matrix is in Table 8. The capability to classify COVID and SARS reads correctly decreases significantly, but the same is not true for adenovirus reads: the number of correctly classified adenovirus reads is higher than in the base case.

Changing Model (= Training Data) Quality. Finally, we consider the effects of decreased model quality resulting from low quality training data. Specifically, before creating the triplet distribution likelihood functions, we subject each of the three genomes to degradation by 2000 iterations of the `Mason_variator`. Figure 7 shows the results. As in the preceding variation, adenovirus suffers more than COVID or SARS. Comparison of the lower panel there with the bottom panel in Figure 6 shows that the effect of poor input data in the former exceeds the effect of poor training data in the latter.

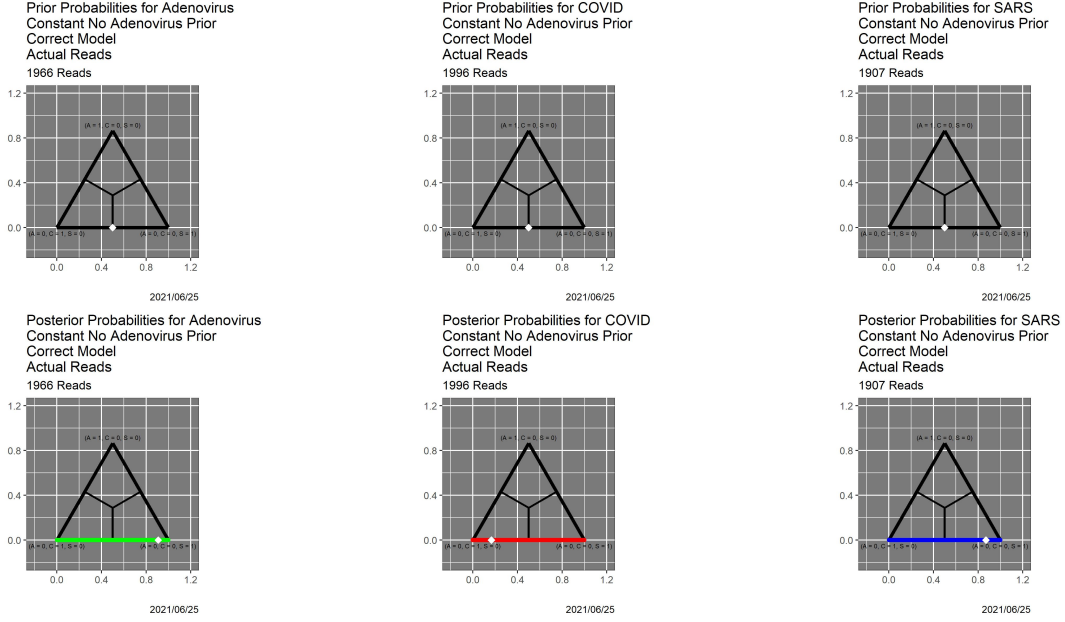
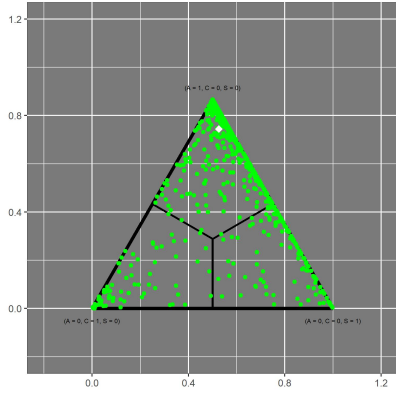


Figure 5: Prior and posterior probabilities for the case of actual reads, “no adenovirus priors” and correct triplet distribution-based models. *Top left:* Prior probabilities for reads from adenovirus. *Top middle:* Prior probabilities for reads from COVID. *Top right:* Prior probabilities for reads from SARS. *Bottom left:* Posterior probabilities for reads from adenovirus. *Bottom middle:* Posterior probabilities for reads from COVID. *Bottom right:* Posterior probabilities for reads from SARS.

	Decision			Sum
	Adeno	COVID	SARS	
Adeno	1827	22	117	1966
COVID	821	644	531	1996
SARS	1042	65	800	1907
Sum	3690	731	1448	5869

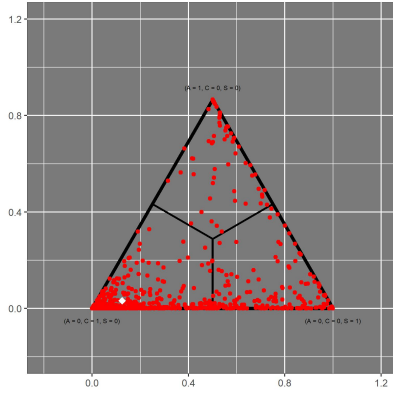
Table 8: Confusion matrix for the MAP classifier for the case of reads degraded by 1000 `Mason_variator` iterations, informative priors, and correct triplet distribution-based model. The correct classification rate is 54.80%

Posterior Probabilities for Adenovirus
Informative Prior
Correct Model
Actual Reads
1966 Reads



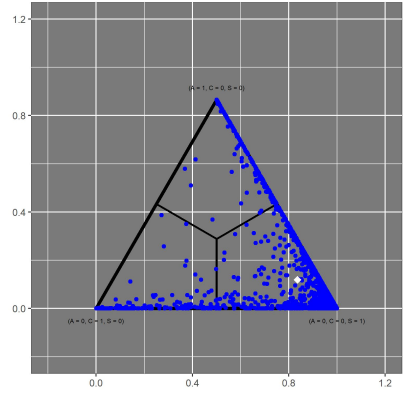
2021/07/13

Posterior Probabilities for COVID
Informative Prior
Correct Model
Actual Reads
1996 Reads



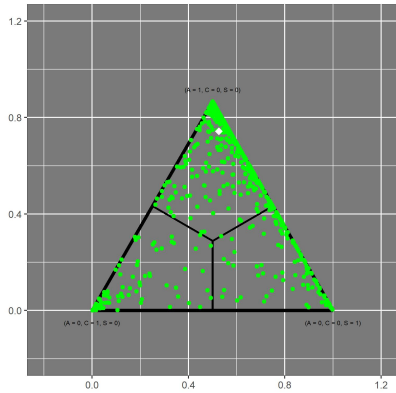
2021/07/13

Posterior Probabilities for SARS
Informative Prior
Correct Model
Actual Reads
1907 Reads



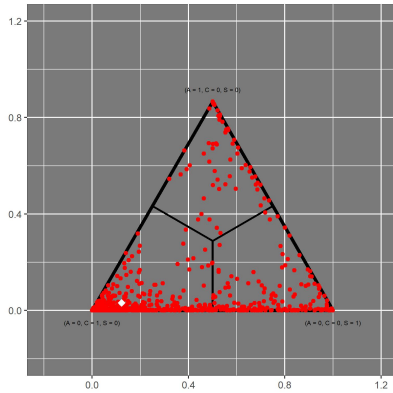
2021/07/13

Posterior Probabilities for Adenovirus
Informative Prior
Correct Model
Error-free Reads
1966 Reads



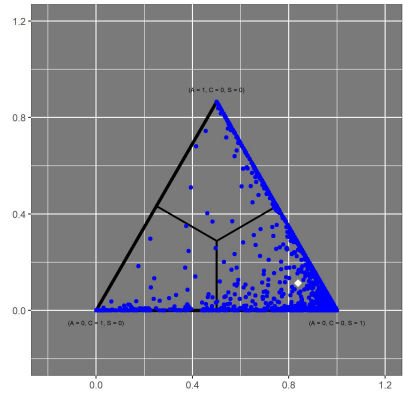
2021/07/13

Posterior Probabilities for COVID
Informative Prior
Correct Model
Error-free Reads
1996 Reads



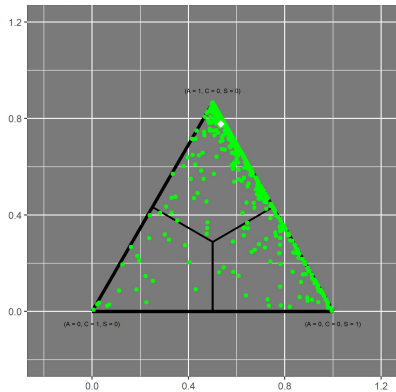
2021/07/13

Posterior Probabilities for SARS
Informative Prior
Correct Model
Error-free Reads
1907 Reads



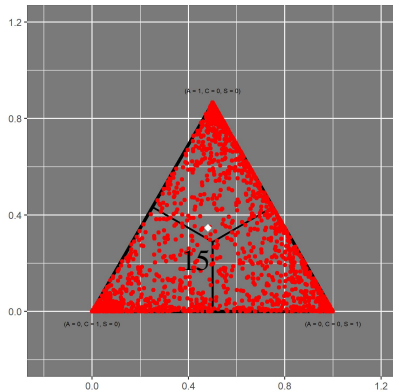
2021/07/13

Posterior Probabilities for Adenovirus
Informative Prior
Correct Model
Degraded Reads (1000 iterations)
1966 Reads



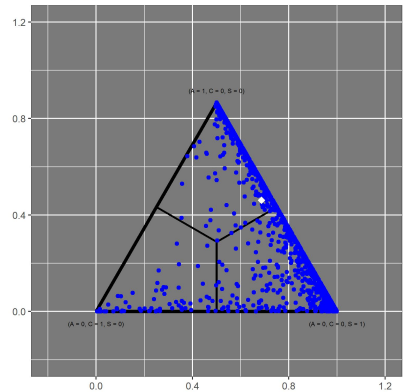
2021/07/20

Posterior Probabilities for COVID
Informative Prior
Correct Model
Degraded Reads (1000 iterations)
1996 Reads



2021/07/20

Posterior Probabilities for SARS
Informative Prior
Correct Model
Degraded Reads (1000 iterations)
1907 Reads



2021/07/20

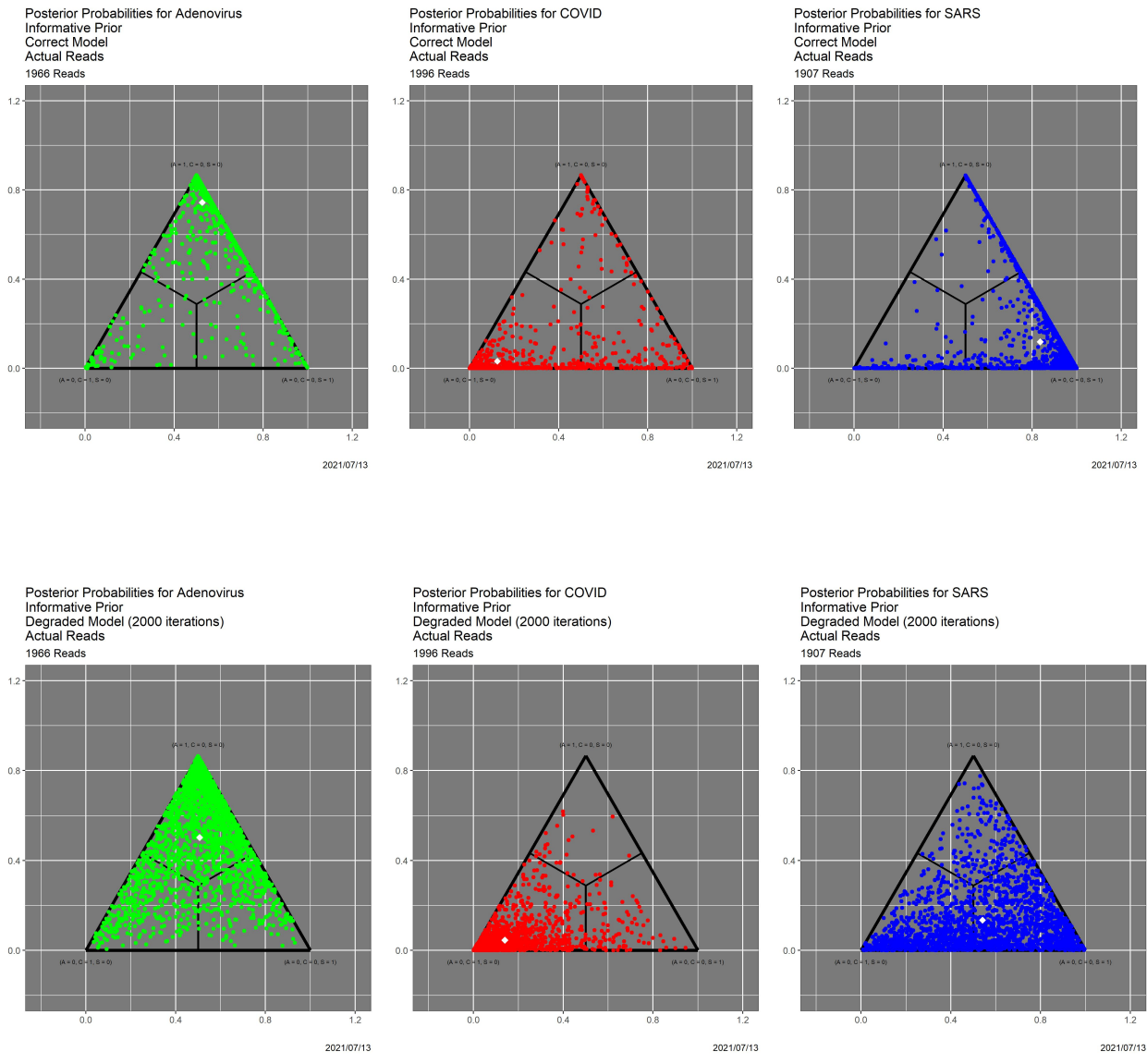


Figure 7: Posterior probabilities showing the effect of low quality models resulting from low quality training data. *Top*: Base case—actual reads, informative priors, correct models. *Bottom*: Actual reads, informative priors, degraded models.

4.4 Detecting Contamination

We sketch here how our strategy can be applied to detect contamination, a major issue in some genomics and metagenomics settings.⁸ To maintain continuity, we use the same three reference genomes as in §4, but with adenovirus viewed as the contaminant.

The key point is addressed in Figure 5: contamination not allowed for in the priors cannot be detected. If we replace the “no adenovirus” priors $\pi_R = (0, 1/2, 1/2)$ underlying Figure 5 by “almost no adenovirus” priors $\pi_R = (0.0001, 0.9999/2, 0.9999/2)$, the result is as shown in Figure 8. For the original task of classifying (roughly comparable numbers of) reads, the performance is noticeably less than in the base case of Figure 3, which is confirmed by comparison of the confusion matrices—that for the base case in Table 5, and that for the case at hand in Table 9. The correct classification rate drops from 86.35% to 62.57%, which is sobering, but not frightening. The performance for COVID and SARS reads is undiminished. Crucial for what follows, the presence of adenovirus reads is confirmed.

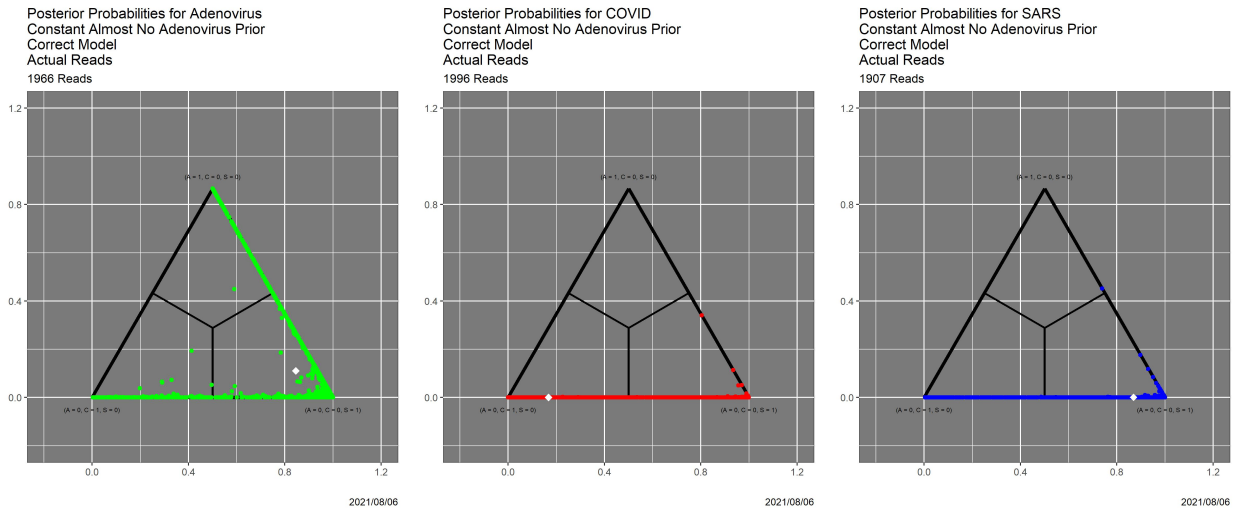


Figure 8: Posterior probabilities for the case of actual reads, “almost no adenovirus priors” and correct triplet distribution-based models. *Left:* Posterior probabilities for reads from adenovirus. *Middle:* Posterior probabilities for reads from COVID. *Right:* Posterior probabilities for reads from SARS.

Can much smaller numbers of adenovirus reads be detected by our methodology? A plausible strategy is to establish a threshold on the posterior probability of adenovirus and to declare, or at least suspect, contamination if sufficiently many—which might be as few as one—adenovirus posterior probabilities exceed that threshold. One candidate for the threshold is the maximum of the adenovirus posterior probabilities

⁸For example, Reich (2018) cites microbial and experimenter contamination as major problems in the context of ancient DNA.

	Decision			
Source	Adeno	COVID	SARS	Sum
Adeno	215	163	1589	1966
COVID	0	1728	268	1996
SARS	1	177	1729	1907
Sum	469	2063	3337	5869

Table 9: Confusion matrix for the MAP classifier for the case of actual reads, “almost no adenovirus” prior and correct triplet distribution-based models. Rows are read sources; columns are MAP decisions. The correct classification rate is 62.57%.

over the $3903 = 1996 + 1907$ COVID and SARS reads in the dataset, which is

$$T^* = \max \{P(\text{Adeno}|\mathbf{R}) : \text{Source}(\mathbf{R}) \neq \text{Adeno}\} = 0.5219, \quad (5)$$

where $p(\cdot|\mathbf{R})$ is the posterior probability given by (4). Note that false positives do not occur if the threshold is greater than T^* , so there is no benefit from using a larger threshold.

Arguably, a traditional receiver operating characteristic (ROC) curve approach (Fawcett, 2006; Karr et al., 2019) is too aggressive; while values of area under the curve (AUC) are high, unless the utility function is skewed, there are too many false positives. Figure 9 points toward an alternative decision strategy. It shows the mean probability of detection, averaged over 2000 replicates, for numbers of contaminating adenovirus reads ranging from 1 to 20, as a function of threshold. The vertical black line is the value T^* given by (5). As noted previously, there are no false positives for thresholds exceeding T^* . For 20 reads, the probability of detecting contamination at this threshold is nearly 0.9, and even for only one read, it still exceeds 0.1.

5 Conclusion

Triplet distributions are the “sweet spot” means of dimension reduction for virus genomes. In the applications to outlier identification and read classification—the major contributions of the paper, the results are not only statistically strong but also scientifically interpretable.

To understand the extent to which these results apply to longer genomes, or larger genome databases, requires further research. Computationally, there are not major impediments: almost all of the tools employed here have memory and running time demands that are linear in genome length and database size. The cluster analyses in §3 are an exception, because they require distance matrices whose size is the square of the database size (divided by 2, of course). The read classification problem is linear in the number of classes and the number of reads. The big question is whether, for instance, a 64- or 21-dimensional summary of a 3 million BP genome (bacteria) or 3 billion BP genome (humans) captures enough information to be both statistically useful and scientifically credible.

Acknowledgements

This research was supported in part by NIH grant 5R01AI100947–06, “Algorithms and Software for the Assembly of Metagenomic Data,” to the University of Maryland College Park (Mihai Pop, PI).

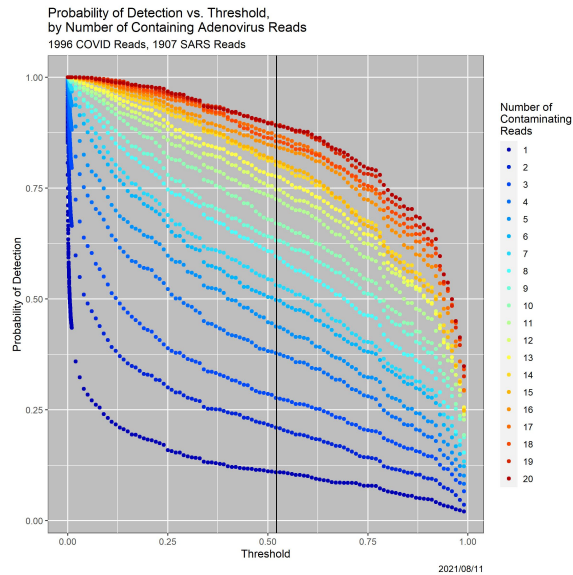


Figure 9: Detection probabilities for adenovirus contamination as a function of threshold and number of contamination reads.

References

- Aggarwal, C. C. and Reddy, C. K., editors (2013). *Data Clustering: Algorithms and Applications*. Chapman and Hall/CRC, London.
- Biggio, B. and Roli, F. (2018). Wild patterns: Ten years after the rise of adversarial machine learning. *Pattern Recognition*, 834:317–331.
- Campbell, A., Mrázek, J., and Karlin, S. (1999). Genome signature comparisons among prokaryote, plasmid, and mitochondrial DNA. *Proceedings of the National Academy of Sciences*, 96(16):9184–9189.
- Cox, T. F. and Cox, M. A. A. (2001). *Multidimensional Scaling*. Chapman and Hall, London.
- Everitt, B. (2011). *Cluster Analysis*. Wiley, Chichester, U.K.
- Fawcett, T. (2006). An introduction to ROC analysis. *Pattern Recognition Letters*, 27(8):861–874.
- Holtgrewe, M. (2010). Mason: A read simulator for second generation sequencing data. *Technical Report FU Berlin*.
- Huang, W., Li, L., Myers, J. R., and Marth, G. T. (2012). ART: a next-generation sequencing read simulator. *Bioinformatics*, 28(4):593–594.
- Karlin, S., Mrázek, J., and Campbell, A. M. (1997). Compositional biases of bacterial genomes and evolutionary implications. *Journal of Bacteriology*, 179(12):3899–3913.

- Karr, A. F., Hauzel, J., Menon, P., Porter, A. A., and Schaefer, M. (2021a). Specified Certainty Classification. Technical report, Fraunhofer Center Mid-Atlantic, Riverdale, MD. arXiv/2109.06677.
- Karr, A. F., Hauzel, J., Porter, A. A., and Schaefer, M. (2021b). Measuring Quality of DNA Sequence Data via Degradation. Technical report, Fraunhofer Center Mid-Atlantic, Riverdale, MD.
- Karr, A. F., Taylor, M. T., West, S. L., Setoguchi, S., Kou, T. D., Gerhard, T., and Horton, D. B. (2019). A comparison of record linkage software and algorithms using real-world data. *PLoS ONE*, 14(9):e0221459.
- Kruskal, J. B. and Wish, M. (1978). *Multidimensional Scaling*. SAGE, New York.
- Müllner, D. (2013). fastcluster: Fast hierarchical, agglomerative clustering routines for R and Python. *Journal of Statistical Software*, 53(9):1–18.
- Nikulin, M. S. (2001). Hellinger distance. In *Encyclopedia of Mathematics*. EMS Press, Berlin.
- Pride, D. T., Meinersmann, R. J., Wassenaar, T. M., and Blaser, M. J. (2003). Evolutionary implications of microbial genome tetranucleotide frequency biases. *Genome Research*, 13:145–158.
- R Core Team (2020). *R: A Language and Environment for Statistical Computing*. R Foundation for Statistical Computing, Vienna, Austria.
- Reich, D. (2018). *Who We Are and How We Got Here: Ancient DNA and the New Science of the Human Past*. Vintage Books, New York.
- Rosen, G., Garbarine, E., Caseiro, D., Polikar, R., and Sokhansanj, B. (2008). Metagenome fragment classification using N-mer frequency profiles. *Advances in Bioinformatics*, 2008(205969):1–12.
- Steinegger, M. and Salzberg, S. L. (2020). Terminating contamination: large-scale search identifies more than 2,000,000 contaminated entries in GenBank. *Genome Biology*, 21(1):115.
- Takashi, A., Shigehiko, K., Makoto, K., Yuta, I., Tokio, K., and Toshimichi, I. (2003). Informatics for unveiling hidden genome signatures. *Genome Research*, 13:693–702.
- Teeling, H., Meyerdierks, A., Bauer, M., Amann, R., and Glöckner, F. O. (2004a). Application of tetranucleotide frequencies for the assignment of genomic fragments. *Environmental Microbiology*, 6(9):938–947.
- Teeling, H., Waldmann, J., Lombardot, T., Bauer, M., and Glöckner, F. O. (2004b). TETRA: a web-service and a stand-alone program for the analysis and comparison of tetranucleotide usage patterns in DNA sequences. *BMC Bioinformatics*, 5(163).
- Valdivia-Granda, W. A. (2019). Big data and artificial intelligence for biodefense: A genomic-based approach for averting technological surprise. In Singh, S. K. and Kuhn, J. H., editors, *Defense Against Biological Attacks*, pages 317–327. Springer-Verlag, New York.
- Wang, Q., Garrity, G. M., Tiedjel, J. M., and Cole, J. R. (2007). Naïve Bayesian classifier for rapid assignment of rRNA sequences into the new bacterial taxonomy. *Applied and Environmental Microbiology*, 73(16):5261–5267.

A Example Triplet and Amino Acid Distributions

Table 10 contains the triplet distributions for the three virus genomes underlying the read classification problem in §4. The corresponding amino acid distributions are in Table 11. We discuss in §4 the extent to which these differ across the three genomes.

Triplet	Adeno	COVID	SARS	Triplet	Adeno	COVID	SARS
AAA	0.031826	0.026367	0.025581	GAA	0.017496	0.012899	0.015261
AAC	0.020016	0.010660	0.018051	GAC	0.012220	0.005982	0.012337
AAG	0.018463	0.016776	0.018891	GAG	0.013832	0.007252	0.013278
AAT	0.018551	0.030176	0.021917	GAT	0.011927	0.021621	0.015597
ACA	0.020016	0.012699	0.026219	GCA	0.017847	0.008221	0.014421
ACC	0.015327	0.006851	0.013076	GCC	0.015063	0.004278	0.007866
ACG	0.010316	0.003709	0.005210	GCG	0.015327	0.002373	0.004975
ACT	0.016265	0.016609	0.022018	GCT	0.016499	0.013868	0.020908
AGA	0.014213	0.016208	0.018085	GGA	0.016704	0.005514	0.011698
AGC	0.017701	0.007519	0.011765	GGC	0.014243	0.005247	0.009849
AGG	0.015591	0.008421	0.013984	GGG	0.012279	0.003409	0.004975
AGT	0.014711	0.019015	0.015059	GGT	0.013041	0.018346	0.013916
ATA	0.012836	0.024429	0.013345	GTA	0.013334	0.020151	0.014723
ATC	0.011224	0.010694	0.011294	GTC	0.010228	0.007419	0.009984
ATG	0.017378	0.029475	0.026085	GTG	0.014067	0.016308	0.018488
ATT	0.018990	0.038765	0.024438	GTT	0.016294	0.037562	0.019698
CAA	0.020573	0.012565	0.024471	TAA	0.018961	0.032148	0.019160
CAC	0.014008	0.006015	0.016202	TAC	0.015679	0.017244	0.019933
CAG	0.019342	0.008956	0.014891	TAG	0.010579	0.018179	0.011832
CAT	0.017115	0.012030	0.018589	TAT	0.012836	0.039533	0.019026
CCA	0.019400	0.006149	0.013311	TCA	0.013774	0.012498	0.020202
CCC	0.014067	0.002573	0.004773	TCC	0.013744	0.006115	0.007059
CCG	0.010257	0.001604	0.003059	TCG	0.008059	0.003676	0.005849
CCT	0.014506	0.009491	0.011631	TCT	0.014301	0.019416	0.019093
CGA	0.009055	0.002406	0.004672	TGA	0.015503	0.023593	0.022018
CGC	0.015503	0.001771	0.004471	TGC	0.017290	0.014203	0.022085
CGG	0.010257	0.001571	0.002756	TGG	0.018170	0.019115	0.018723
CGT	0.009143	0.005614	0.007194	TGT	0.017027	0.038464	0.026724
CTA	0.013012	0.017544	0.018723	TTA	0.018873	0.044981	0.023160
CTC	0.011459	0.007085	0.012000	TTC	0.016968	0.016508	0.018925
CTG	0.017525	0.014203	0.018891	TTG	0.019019	0.035390	0.026085
CTT	0.019576	0.020552	0.024034	TTT	0.030595	0.059985	0.027463

Table 10: Triplet distributions for the adenovirus, COVID and SARS genomes underlying §4.

Amino Acid	Adeno	COVID	SARS
Alanine	0.043959	0.011362	0.019093
Arginine	0.092782	0.054271	0.074322
Asparagine	0.037892	0.080370	0.049245
Aspartate	0.030537	0.031747	0.037615
Cysteine	0.030331	0.016408	0.031430
Glutamate	0.031035	0.027637	0.036035
Glutamine	0.024294	0.023727	0.028472
Glycine	0.058231	0.019817	0.032774
Histidine	0.029628	0.057713	0.034421
Isoleucine	0.042376	0.089861	0.050018
Leucine	0.094042	0.088591	0.096440
Lysine	0.047563	0.076494	0.046388
Methionine; START	0.015679	0.017244	0.019933
Phenylalanine	0.050289	0.043143	0.044472
Proline	0.056267	0.032516	0.040438
Serine	0.084049	0.067337	0.084944
STOP	0.046479	0.066067	0.057750
Threonine	0.067989	0.095375	0.089549
Tryptophan	0.015327	0.006851	0.013076
Tyrosine	0.030214	0.053903	0.039430
Valine	0.071037	0.039567	0.074154

Table 11: Amino acid distributions for the adenovirus, COVID and SARS genomes underlying §4.